2005-05

Deformation mechanisms in superplastic AA5083 materials

Kulas, Mary-Anne; Green, W. Paul; Taleff, Eric M.; Krajewski, Paul E.; McNelley, Terry R.

M.-A. Kular, W.P. GReen, E.M. Taleff, P.E. Karjewski, T.R. McNelley, "Deformatin mechanisms in superplastic AA5083 materials," Metallurgical and Materials Transaction A.,v.36A, (May 2005), p. 1249-1261.
https://hdl.handle.net/10945/55368

Deformation Mechanisms in Superplastic AA5083 Materials

MARY-ANNE KULAS, W. PAUL GREEN, ERIC M. TALEFF, PAUL E. KRAJEWSKI, and TERRY R. McNELLEY

The plastic deformation of seven 5083 commercial aluminum materials, produced from five different alloy heats, are evaluated under conditions of interest for superplastic and quick-plastic forming. Two mechanisms are shown to govern plastic deformation in AA5083 over the strain rates, strains, and temperatures of interest for these forming technologies: grain-boundary-sliding (GBS) creep and solute-drag (SD) creep. Quantitative analysis of stress transients following rate changes clearly differentiates between GBS and SD creep and offers conclusive proof that SD creep dominates deformation at fast strain rates and low temperature. Furthermore, stress transients following strain-rate changes under SD creep are observed to decay exponentially with strain. A new graphical construction is proposed for the analysis and prediction of creep transients. This construction predicts the relative size of creep transients under SD creep from the relative size of changes in an applied strain rate or stress. This construction reveals the relative size of creep transients under SD creep to be independent of temperature; temperature dependence resides in the "steady-state" creep behavior to which transients are related.

I. INTRODUCTION

THE transportation industry and the automotive industry, in particular, have made increasing use of aluminum alloys in new vehicle construction.[1–4] The primary incentive for using aluminum is the reduction in vehicle mass, which it makes possible. In automotive applications, mass reduction improves performance and fuel economy. An important factor limiting the introduction of aluminum sheet materials into vehicle components, such as body closure panels, is low formability in cold stamping operations. Steel sheet materials can provide elongations of up to 50 pct, while aluminum sheet materials typically provide a maximum of 30 pct. Superplastic aluminum sheet material offers a potential solution to this dilemma. Superplasticity is the ability of a material to exhibit very high tensile ductility, from a few hundred percent to thousands of percent, typically at elevated temperatures and slow strain rates.[5] Two requirements exist for a material to be superplastic: (1) a high strain-rate sensitivity is necessary to reduce the rate of flow localization, i.e., necking, and (2) a low rate of damage accumulation, e.g., cavitation, is necessary to allow large plastic strains to be reached.

The deformation mechanism generally accepted as responsible for fine-grain superplasticity in aluminum alloys is grain-boundary-sliding (GBS) creep, which supplies a high strain-rate sensitivity (m $\sim$ 0.5) while producing the low flow stress typically necessary for successful commercial superplastic forming (SPF) operations.[6–15] Aluminum alloy 5083 is the most common material in SPF operations, and it deforms by GBS creep at the elevated temperatures and slow strain rates typical of SPF operations.[16–21] AA5083 also offers the additional benefits of moderate strength, good weldability, and acceptable corrosion resistance, which make it of prime interest for application to new vehicle construction.[16] More recently, data have been presented that suggest AA5083 deforms by solute-drag (SD) creep at temperatures below and strain rates faster than those at which GBS creep dominates deformation.[17,19,22–25] The present investigation offers conclusive proof that this is, indeed, the case. The SD creep produces a high strain-rate sensitivity ($m \sim 0.33$ to 0.25), although not as high as that of GBS creep, and can provide very good tensile ductility.[26–34] A proprietary variation on SPF, called quick-plastic forming (QPF), takes advantage of SD creep in AA5083 to increase forming rates and decrease forming temperatures in comparison with those historically used for SPF operations.[2] The QPF technology has made possible the commercial forming of complex parts in large quantities and at fast production rates.[2,4]

The introduction of AA5083 parts made by SPF or QPF into new vehicles is limited by two economic factors, material cost and production cost. Fortunately, there is the promise of technological solutions for each of these issues. Superplastic-grade AA5083 material is typically produced by direct-chill (DC) casting. However, significant cost savings are possible if superplastic AA5083 grades can be produced by continuous casting (CC). For this technology to be realized, the superplastic performance of AA5083 materials produced by CC must be better understood. Many of the costs in SPF operations are associated with high temperatures and slow production rates. Cost reduction in SPF and QPF operations may be achieved if AA5083 materials can be formed at low temperatures and fast strain rates. The means of reaching this goal historically proposed by researchers is to reduce the recrystallized grain size of AA5083 materials, which will push deformation by GBS creep, and the superplastic response, to lower temperatures and faster strain rates. However, current techniques that significantly reduce the recrystallized grain size in AA5083 introduce substantial expense, either through additional processing or through expensive alloying additions, such as Sc.[16,35–40] A more promising proposal is the use of small alloying changes to

MARY-ANNE KULAS, Materials Science and Engineering Program, and W. PAUL GREEN and ERIC M. TALEFF, Department of Mechanical Engineering, are with the University of Texas at Austin, Austin, TX 78712-0292. Contact e-mail: taleff@mail.utexas.edu PAUL E. KRAJEWSKI is with the Research and Development Center, General Motors Corp., Warren, MI 48090-9056. TERRY R. McNELLEY is with the Department of Mechanical Engineering, Naval Postgraduate School, Monterey, CA 93943-5146.

Manuscript submitted August 26, 2004.

enhance GBS creep deformation, but this alternative still needs fundamental investigation before reaching practical use.[41,42] The recent production successes of QPF technology support the idea that SD creep, which controls deformation in AA5083 at temperatures below and strain rates above those for which GBS creep controls deformation, may be used to increase forming rates and decrease forming temperatures. In order to use SD creep, where necessary, and GBS creep, where possible, a better understanding of the relationships between these two deformation mechanisms in AA5083 must be established.

Six superplastic-grade AA5083 sheet materials and one hot-rolled AA5083 plate, which represent five different alloy heats, are evaluated in the present investigation. The hot-rolled AA5083 plate was produced from a DC casting. Among the six sheet materials, five were produced from DC castings and one was produced by a CC operation. Two of the AA5083 sheet materials were cold rolled from the hot-rolled AA5083 plate studied; these are products of the same alloy heat. The chemical compositions of the five alloy heats studied are quite similar. These materials were selected because they produce widely different usable ductilities in forming operations, making an understanding of the mechanisms governing their elevated-temperature deformation of particular interest. Ductility data are not discussed here, but will be detailed in a subsequent article. All the materials were subjected to mechanical testing at elevated temperatures in order to specifically determine the deformation mechanisms active in each over a range of temperatures and strain rates. Optical microscopy was conducted to observe the recrystallized microstructure of each material and to determine grain sizes before and after deformation by mechanical testing.

II. EXPERIMENTAL PROCEDURE

Compositions of the five different AA5083 alloy heats investigated are given in Table I as weight percent. In the naming convention of Table I, DC indicates a DC-cast material and CC indicates a continuously cast material. Alloy DC-D is investigated in three different forms: DC-D-HB is a hot-band material from the hot rolling process used prior to cold rolling in superplastic sheet production; DC-D-1.6 is a material cold rolled from the DC-D-HB material to a thickness of 1.6 mm; and DC-D-1.2 is a material cold rolled from the DC-D-HB material to a thickness of 1.2 mm. All five alloys have very similar compositions, but each of the seven materials derived from these alloys was produced using different thermomechanical processing schedules. The DC materials were produced by hot-and-cold rolling of homogenized castings, and each was produced using a slightly different rolling schedule. The total cold-rolling reduction imposed on each material is listed in Table I as a true strain. Materials in this study were provided by Pechiney Rolled Products (Ravenswood, WV); Arco Aluminum, Inc. (Louisville, KY); and Commonwealth Aluminum Corp. (Uhrichsville, OH).

Two "dog-bone" specimen geometries were used for mechanical testing of the AA5083 sheet materials, one with a gage length of 25.4 mm and the other with a gage length of 50.8 mm. Both geometries used the as-received thickness of the material, a gage width of 6.0 mm, and a shoulder radius of 7.9 mm. The sheet rolling direction was always oriented parallel to the tensile axis. Specimens were tested using rigid, shoulder-loading grips, which effectively prevent measurable plastic deformation within the sample grip region. This rigid grip design allows for accurate measurement of elongation from grip displacement; the accuracy of this technique increases with specimen gage length. Mechanical tests were performed at temperatures from 425 °C to 500 °C and strain rates from 3×10^{-5} to 1×10^{-1} s^{-1}. Temperature was controlled to within ± 1 °C along each specimen gage length using a resistance furnace with three independent heating zones. Thermocouples contacting each specimen at the extremes of its gage length were used to verify temperature uniformity during mechanical tests. Specimens were tested at constant crosshead speeds in a screw-driven, computer-controlled, electromechanical testing machine to impose prescribed strain rates. Two types of mechanical tests were conducted, strain-rate-change (SRC) tests and transient-behavior (TB) tests.

Strain-rate-change tests were conducted at elevated temperatures for each material. The SRC tests use a series of strain rates imposed upon a single specimen, with each rate held for a minimum of 2 pct engineering strain, to produce data for flow stress as a function of temperature, strain, and strain rate. "Steady-state" flow stress measurements were made after each rate change by evaluating the stress transient following the rate change and measuring the stress at which the transient had fully decayed. Each SRC specimen was initially prestrained to approximately 15 pct engineering strain to ensure that the specimen was well seated in the grips and that its microstructure had stabilized. Following this prestrain step, seven sequential steps of increasing strain rate were imposed, with rates varying from low, 3×10^{-5} s^{-1}, to high 3×10^{-2} s^{-1}. After this series, two additional steps were imposed to repeat rates from the initial series, as a check on the repeatability of flow stress measurements. The SRC tests were con-

Table I. Sheet Thickness, t, Total Strain from Cold Rolling, ε_{cr}, and Composition of Each AA5083 Material

Material	t (mm)	ε_{cr}	Composition (Wt Pct)						
			Si	Fe	Cu	Mn	Mg	Cr	Al
DC-A	1.4	−1.3	0.09	0.21	0.04	0.86	4.71	0.10	bal
DC-B	1.6	−1.3	0.06	0.11	0.01	0.78	4.69	0.06	bal
DC-C	1.2	−1.3	0.15	0.20	0.03	0.76	4.50	0.07	bal
DC-D-HB	4.8	0.0	0.10	0.24	0.04	0.89	4.80	0.13	bal
DC-D-1.6	1.6	−1.1	0.10	0.24	0.04	0.89	4.80	0.13	bal
DC-D-1.2	1.2	−1.4	0.10	0.24	0.04	0.89	4.80	0.13	bal
CC-A	1.0	−1.6	0.07	0.22	0.02	0.72	4.70	—	bal

ducted at temperatures of 425 °C, 450 °C, 475 °C, and 500 °C for each material, except those of the DC-D alloy, which were tested only at 450 °C. A set of specialized SRC tests, referred to herein as TB tests, were used to investigate stress transients following strain-rate changes. The TB tests, such as SRC tests, imposed an initial prestrain of approximately 15 pct engineering strain on each test specimen. After this prestrain, a number of large positive or negative strain-rate changes were imposed, and each new rate was held to the strain necessary for nearly complete decay of the resulting stress transient. Large strain-rate changes produced large transients in flow stress, and the resulting stress transients were quantitatively evaluated for size and rate of decay with strain.

Grain size was measured for all materials after recrystallization by taking metallographic specimens from the grip (undeformed) and gage (deformed) regions of SRC specimens tested at a temperature of 450 °C. Grain sizes measured in grip sections represent statically recrystallized grain sizes, while those measured in gage sections after testing are expected to reveal any dynamic grain growth. Grain-size measurements for all materials were performed by observing specimens after mechanical polishing and etching. Etching was performed using one of two different techniques. In the first technique, polished specimens of alloys DC-A, DC-B, DC-C, and CC-A were electrolytically etched in Barker's reagent (1.87 pct flouroboric acid and 98.2 pct H_2O) under a voltage of 25 V for 2 minutes, with the specimen as the anode and a steel plate as the cathode. Specimens thus prepared were examined in an optical microscope under polarizing filters, which reveal color contrast between grains. In the second technique, metallographic specimens of alloy DC-D were aged at 150 °C for 24 hours to sensitize grain boundaries for chemical attack; this effect has been attributed to Mg segregation to boundaries[43] and, alternatively, to precipitation at boundaries.[44] The specimens were then polished and immersed in a solution of 10 pct phosphoric acid at 50 °C with mild agitation to preferentially etch grain boundaries. Specimens thus prepared were examined in an optical microscope bright field. Images for grain-size measurement of alloys DC-A, DC-B, DC-C, and CC-A were digitally acquired at 500 times magnification using a digital image size of 1280 × 1024 pixels, which corresponds to a physical area of 208 × 166 μm. Images for grain-size measurement of alloy DC-D in its three different forms studied were digitally acquired at 600 times magnification using a digital image size of 1280 × 1000 pixels, which corresponds to a physical area of 218 × 170 μm. A minimum of five images was acquired for grain-size measurements at each position (grip and gage) in each material, and the images were analyzed manually using the ASTM E112 standard.[45]

III. RESULTS AND DISCUSSION

A. *SRC Test Results*

Data from SRC tests on materials DC-A, DC-B, DC-C, and CC-A at temperatures from 425 °C to 500 °C are shown in Figure 1. These data are presented as plots of the logarithm of true-strain rate, $\dot{\varepsilon}$, *vs* true steady-state flow stress, σ, compensated by the dynamic, unrelaxed, Young's elastic modulus, E. Temperature-dependent elastic modulus values are taken from the following fit to the data of Köster for pure Al:[46]

$$E = 77{,}630 + 12.98\,T - 0.03084\,T^2 \qquad [1]$$

where E is in MPa, and T is absolute temperature in Kelvin. Data from SRC tests on the materials DC-D-HB, DC-D-1.6, and DC-D-1.2 at 450 °C are presented in a similar manner in Figure 2. The slope of data on these plots is equivalent to the stress exponent, n, from the phenomenological equation for creep. The phenomenological equation for creep can be written as[5]

$$\dot{\varepsilon} = A\left(\frac{\mathbf{b}}{d}\right)^p\left(\frac{\sigma}{E}\right)^n \exp\left(-\frac{Q_c}{\mathrm{R}T}\right) \qquad [2]$$

where A is a constant that depends on the material and the dominant deformation mechanism, $\mathbf{b}$ is the magnitude of the Burgers vector, d is the grain size, p is the grain-size exponent, Q_c is the activation energy for creep, R is the universal gas constant, and the remaining terms are as previously defined.

Values of the stress exponent evidenced by the data of Figures 1 and 2 were measured at the temperatures 450 °C and 500 °C. The measurement method was as follows. Flow stress data for a given material were taken from the SRC test data at three consecutive rates and a constant temperature. These three data were subjected to linear regression on the dual-logarithmic scales shown in Figures 1 and 2. The slope of the resulting line was taken as the stress exponent, n, at the central strain rate. Thus, the stress exponent was not measured at the fastest and slowest strain rates, but was measured at all intermediate rates for which data were available. The resulting measurements for the stress exponent are reported in Figure 3 as plots of stress exponent *vs* the logarithm of strain rate at (a) 450 °C and (b) 500 °C. Stress exponents were measured for all seven materials at 450 °C (Figure 3(a)). At 500 °C (Figure 3(b)), data are not available to calculate stress exponents of the DC-D materials.

At 450 °C, Figure 3(a) reveals the following behaviors in the stress exponent. The DC-D-HB material exhibits n values which decrease from 4.1 to 3.3 with decreasing strain rate. These are consistent with n values observed in coarse-grained Al-Mg-Mn and commercial 5000-series aluminum materials deforming by SD creep at similar temperatures and strain rates[19,25,33,34] and with the relatively coarse recrystallized grain size of the DC-D-HB material (Table II). The remaining AA5083 materials contain fine recrystallized grains. The fine-grained materials exhibit n values in the range of 3.8 to 4.0 at the highest rate, 10^{-2} s^{-1}, suggesting that these materials may also deform by SD creep at this rate. The n values of the fine-grained materials decrease with decreasing strain rate to minimums in the range of 2.4 to 2.7, suggesting a transition to GBS creep in all the fine-grained materials.[5,15] Upon further decrease in strain rate, material CC-A produces an increase in n, which is characteristic of a slight threshold stress behavior. Figure 3(b) exhibits similar behavior at 500 °C. Here, the maximum n values at 10^{-2} s^{-1} are similar, within the range of 3.6 to 3.9. The minimum n values range from 2.1 to 2.3, which are slightly less than those at 450 °C. The DC materials exhibit a slight increase in n at the lowest rate, which indicates a slight effect of threshold stress. The CC-A material, however, exhibits a more significant increase in n at the lowest strain rate, indicating a notable threshold

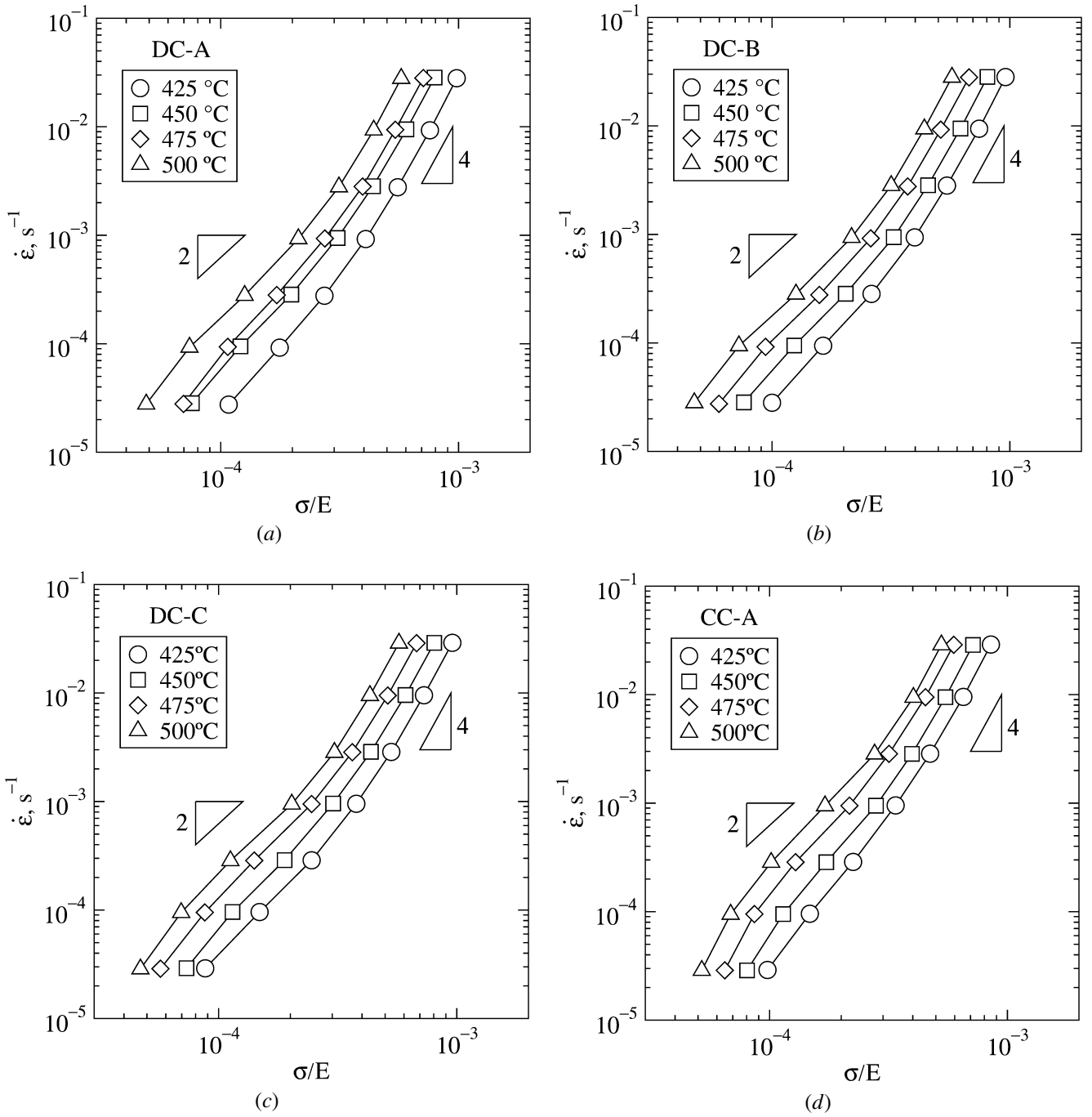

Fig. 1—The results of SRC tests at temperatures from 425 °C to 500 °C are presented as plots of the logarithm of strain rate *vs* the logarithm of modulus-compensated stress for materials (*a*) DC-A, (*b*) DC-B, (*c*) DC-C, and (*d*) CC-A.

stress at 500 °C. The stronger effect of threshold stress in the CC material might be associated with the known effect of impurities at grain boundaries on threshold behavior.[47]

The vertical separation between data at different temperatures, but at constant grain size and constant σ/E, in Figure 1 is proportional to the activation energy for creep. The activation energy for creep, Q_c, can be calculated from SRC data using the following relationship:[48]

$$Q_c = -\mathrm{R}\left.\frac{\partial \ln \dot{\varepsilon}}{\partial 1/T}\right|_{\sigma/E} \qquad [3]$$

Equation [3] indicates that Q_c can be calculated from semilogarithmic plots of strain rate, taken at constant values of σ/E, *vs* inverse temperature. Such plots are presented in Figure 4 for materials (a) DC-A, (b) DC-B, (c) DC-C, and (d) CC-A using the SRC data presented in Figure 1. Because the DC-D materials were tested at only one temperature, their activation energies cannot be calculated. The activation energies calculated by linear regression of the data in Figure 4 are presented in parentheses in Figure 4 along with the (±) standard error, both in units of kJ/mole. The activation energies for all materials with data available in Fig-

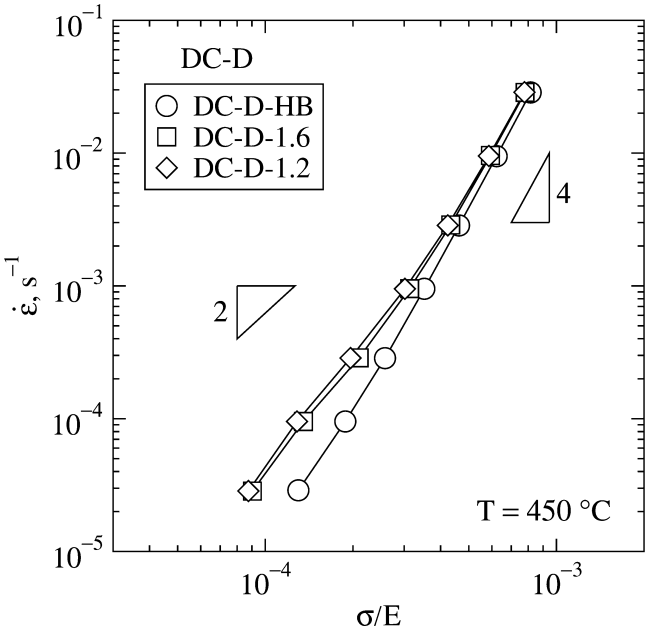

Fig. 2—The results of SRC tests at 450 °C are presented as a plot of the logarithm of strain rate *vs* the logarithm of modulus-compensated stress for materials DC-D-HB, DC-D-1.6, and DC-D-1.2.

ure 4 are within the range of 101 to 135 kJ/mole. The calculated values of activation energy are presented in Figure 5 as a function of the logarithm of modulus-compensated stress. At the highest value of σ/E (6×10^{-4}), all materials have very similar activation energies, within the range of 123 to 135 kJ/mole. This is near the value of approximately 136 kJ/mole previously reported for the activation energy associated with deformation of Al-Mg alloys by SD creep,[49–52] which is consistent with n values reported in Figure 3. At the intermediate value of σ/E (3×10^{-4}), the activation energy for creep drops to within the range of 101 to 109 kJ/mole for all four materials, and it remains constant with decreasing σ/E in the DC materials, to within the standard error of measurements. This is consistent with the low activation energies sometimes observed during deformation by GBS creep when grain-boundary diffusion actively participates.[5] At the lowest value of σ/E (10^{-4}), activation energy increases significantly for the CC-A material. This increase is associated with the threshold behavior noted previously. The activation energies calculated at $\sigma/E = 10^{-4}$ should be considered as apparent activation energies. Calculation of true activation energies for creep is possible by compensation for the threshold stress, but is not demonstrated here because of the modest effect of threshold stress in all but the CC-A material.

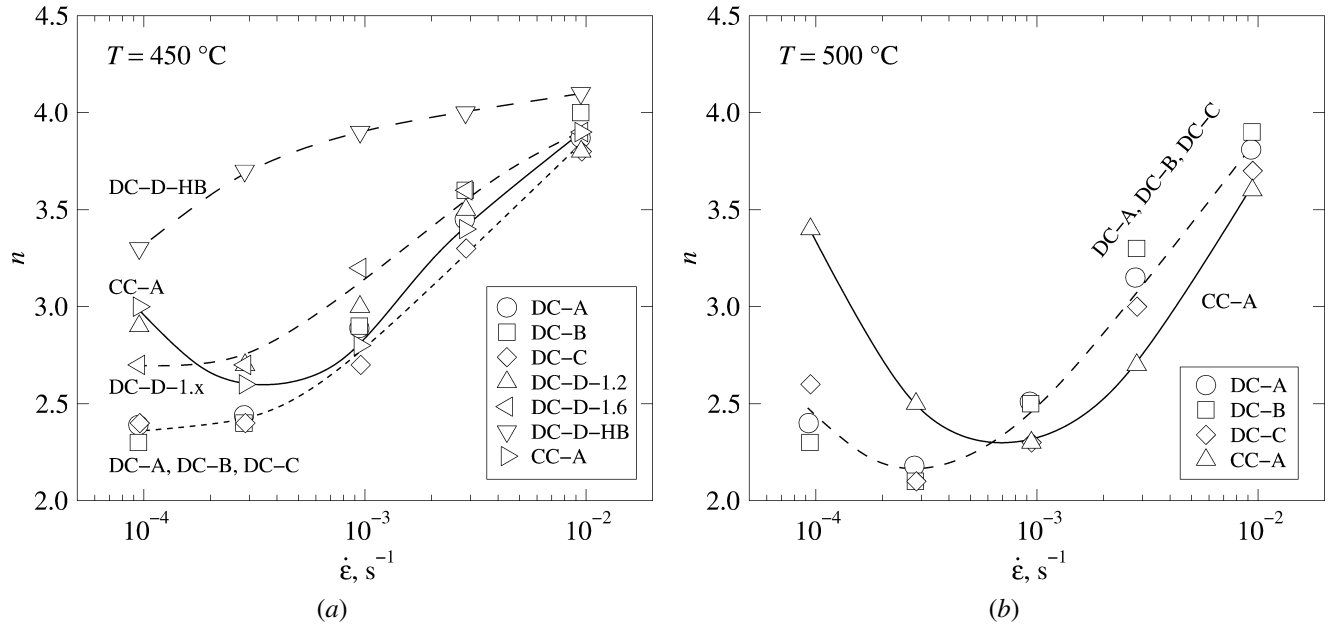

Fig. 3—Stress exponents, n, calculated from SRC data are presented on plots against the logarithm of strain rate at temperatures of (*a*) 450 °C and (*b*) 500 °C.

Table II. Mean-Lineal-Intercept-Length Grain Size after SRC Testing at 450 °C in Specimen Grip (Undeformed) and Gage (Deformed) Regions and Standard Deviations (±SD) of the Measurements

	DC-A	DC-B	DC-C	DC-D-HB	DC-D-1.6	DC-D-1.2	CC-A
l_{grip} (μm)	6.9 ± 0.3	6.6 ± 0.2	6.5 ± 0.4	9.7 ± 0.8	8.2 ± 0.7	7.0 ± 0.6	8.0 ± 0.3
l_{gage} (μm)	6.7 ± 0.2	7.1 ± 0.5	7.0 ± 0.5	10.8 ± 0.4	8.7 ± 0.4	7.2 ± 0.4	7.7 ± 0.3

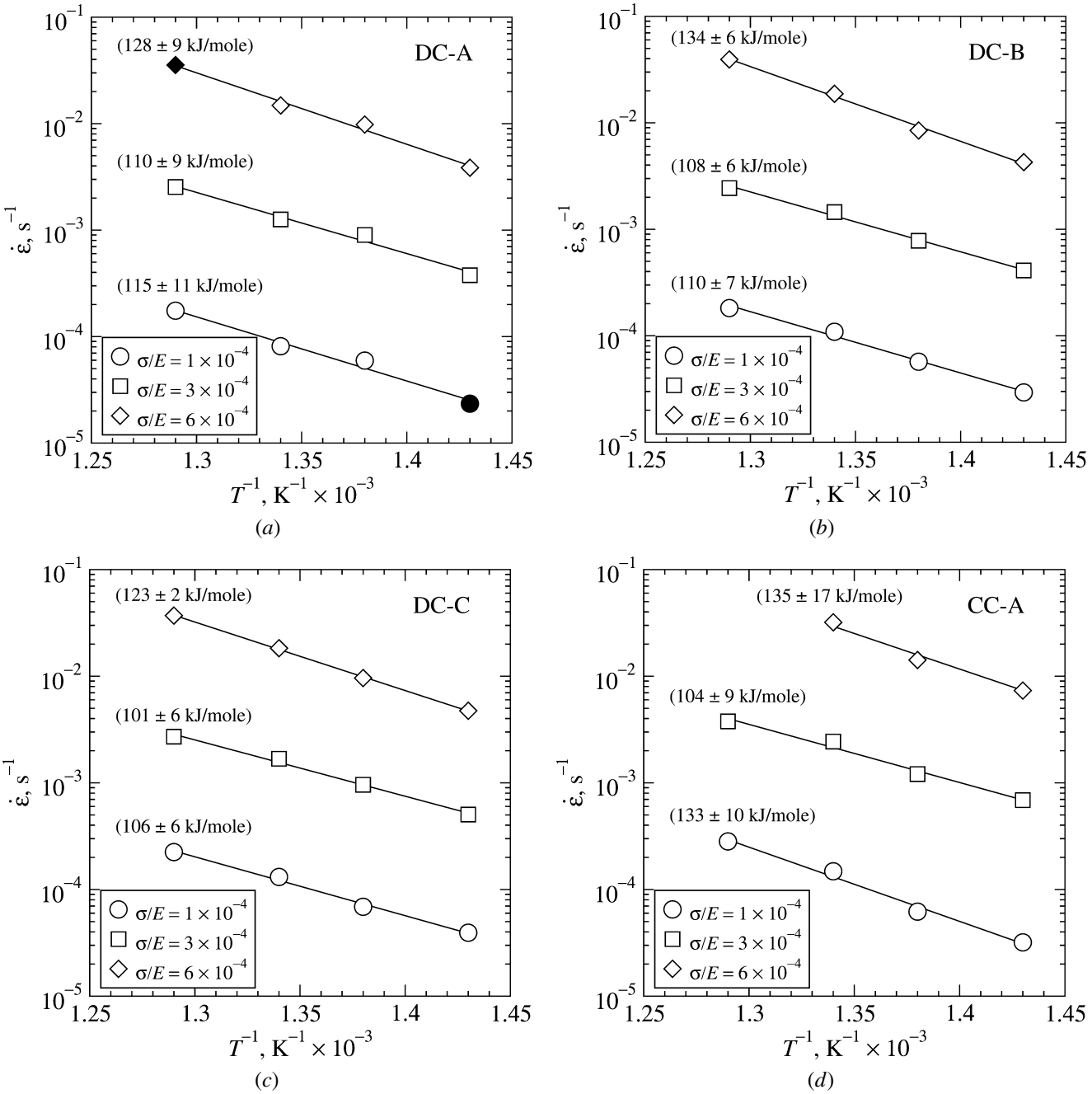

Fig. 4—The logarithm of strain rate is plotted against the inverse absolute temperature at three values of modulus-compensated stress for materials (*a*) DC-A, (*b*) DC-B, (*c*) DC-C, and (*d*) CC-A. Data are taken from the SRC results in Fig. 1, and filled symbols indicate values of strain rate calculated by extrapolating slightly beyond the strain rates for which data are available. Activation energies calculated from the slopes of the data are shown as kJ/mole with the standard errors of the calculated values.

B. *Grain-Size Measurement*

Grain size was measured from specimens after SRC testing at 450 °C both within grip sections, which were not subject to deformation, and within gage sections, which were deformed during testing. Examples of microstructures taken from undeformed grip regions for grain-size measurements are shown in Figures 6(a) and (b) for the DC-B and DC-D-1.2 materials, respectively. Table II shows grain sizes as mean-lineal-intercept lengths for each material after SRC testing at 450 °C in both the grip (undeformed) and gage (deformed) sections. Static recrystallization and grain growth experiments using several of the DC materials (DC-A, DC-B, DC-D-1.2, and DC-D-1.6), studied with orientation-imaging microscopy, indicate that static recrystallization occurs within 5 minutes at 450 °C and that static grain growth within the maximum times required for SRC tests is within the error of grain-size measurements.[53,54] These results indicate that grain sizes measured within the grip (undeformed) section after SRC testing can be considered equivalent to the recrystallized grain size of the material. The recrystallized grain size in the DC-D-HB material is the coarsest, at 9.7 μm, as is expected from the lack of cold rolling in this material. However, it is interest-

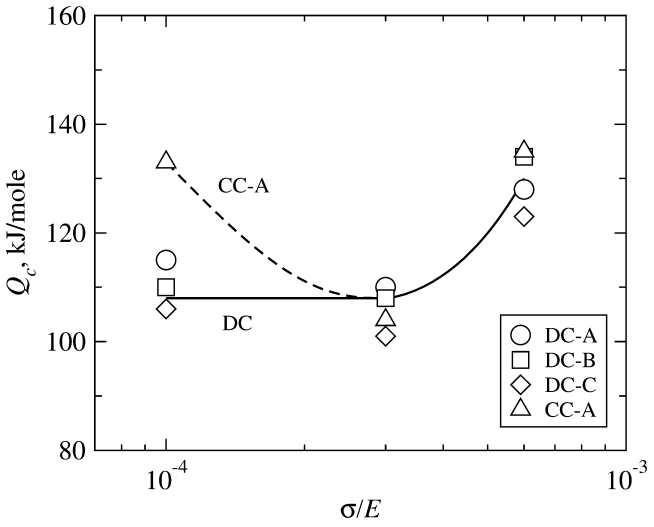

Fig. 5—Activation energies for creep are plotted against the logarithm of modulus-compensated flow stress.

ing to note that this value of 9.7 μm is smaller than might by typically expected of hot-rolled 5000-series aluminum. The recrystallized grain sizes of all the DC cast materials subjected to cold rolling are quite similar and are within the range of 6.5 to 8.2 μm in the grip (undeformed) region after testing; the recrystallized grain size of the DC-D-1.6 material is slightly larger than those of the other DC materials. Comparison of grain sizes between grip (undeformed) and gage (deformed) sections indicates that some dynamic grain growth may have occurred during testing, but such growth is within the standard deviation of the grain-size measurements. Except for the DC-D-HB material, all the AA5083 materials in this investigation possess fine grain sizes of approximately 7 μm.

C. *Deformation Mechanism Maps*

The mechanical testing and microstructural evaluation conducted on the AA5083 materials enables a quantitative description of steady-state deformation within the range of temperatures, strain rates, and grain sizes evaluated. Data from SRC tests of each AA5083 material have been used to develop predictive equations for deformation behavior based upon the phenomenological equation for creep (Eq. [2]) with the inclusion of a term for threshold stress, σ_{th}. The resulting modified equation is of the following form:

$$\dot{\varepsilon} = A\left(\frac{\mathbf{b}}{d}\right)^{p}\left(\frac{\sigma - \sigma_{th}}{E}\right)^{n}\exp\left(-\frac{Q_c}{\mathrm{R}T}\right) \qquad [4]$$

where A is a material constant. The magnitude of the Burgers vector is taken as $\mathbf{b} = 2.86 \times 10^{-10}$ m.[55] The values of A, p, n, and Q_c are expected to be unique for each active deformation mechanism. Equation [4] was fit to the SRC data of each AA5083 material for each active deformation mechanism. The activation energies for the SD and GBS creep mechanisms are $Q_{SD} = 136$ kJ/mole and $Q_{\mathrm{GBS}} = 110$ kJ/mole, respectively. The limited SRC data available at high temperatures and slow strain rates were used to measure the threshold stress of each material in the GBS regime. All fine-grained DC materials exhibit a small threshold stress of approximately 0.7 MPa. The threshold stress of the CC-A material was measured to be approximately 1.7 MPa. The SRC data are not sufficient to determine the temperature dependence of threshold stress. No threshold stress was observed under SD creep conditions. The grain-size exponent, p, is zero under SD creep[33] and is in the range of 2 to 3 under GBS creep;[56] a value of $p = 2$ was assumed under GBS creep for fitting Eq. [4] to data. The grain size of all the fine-grained materials was taken from Table II to be approximately 7 μm; the grain size of the DC-D-HB material was not needed in fitting since its data demonstrate only deformation controlled by SD creep.

Equation [4] was fit by linear regression to data from each deformation mechanism for the DC materials. Independent fits were conducted for the CC-A material, which clearly exhibits a slight difference in behavior from the DC materials. The A and n values calculated from these fits of Eq. [4] are provided in Table III along with the values of other parameters used. Applying the parameters listed in Table III to Eq. [4] produces predictive functions for steady-state creep

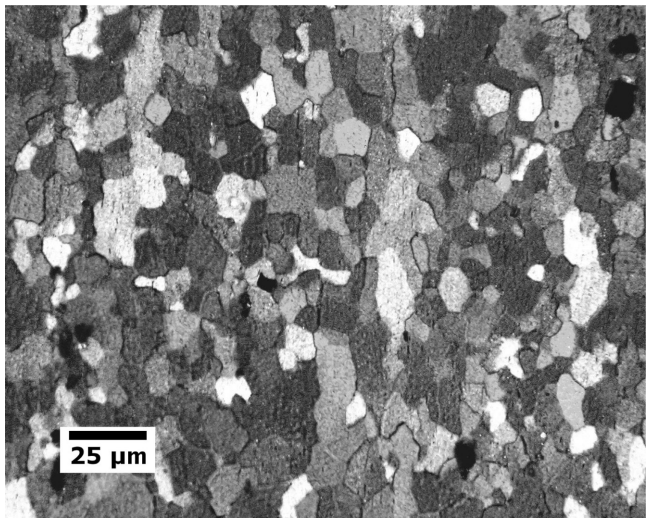

(*a*)

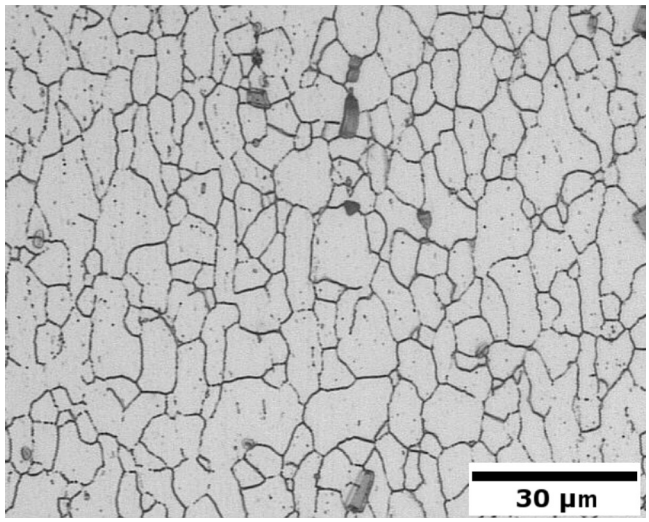

(*b*)

Fig. 6—Typical recrystallized, undeformed microstructures are shown for (*a*) material DC-B, etched using Barker's reagent and viewed under polarizing filters, and (*b*) material DC-D-1.2, etched using a phosphoric acid solution.

Table III. Parameters Determined for Predictive Equations Based on Equation [4]

Material	Mechanism	A (s^{-1})	p	σ_{th} (MPa)	n	Q_c (kJ/mole)
DC	SD	2×10^{20}	0	0	3.9	136
	GBS	1.3×10^{21}	2	0.7	2.1	110
CC-A	SD	8×10^{20}	0	0	4.0	136
	GBS	2.6×10^{20}	2	1.7	1.9	110

rate. These equations allow the prediction of which mechanism will govern deformation at a specific temperature, stress, and grain size. Because SD and GBS are competitive creep mechanisms, the governing deformation mechanism is that which provides the most rapid creep rate, *i.e.*, $\dot{\varepsilon} = \max(\dot{\varepsilon}_{SD}, \dot{\varepsilon}_{GBS})$, until power-law breakdown (PLB) occurs. In developing a global predictive relation, PLB was taken to occur when $\dot{\varepsilon}/D > 10^{13}$ m^{-2},[57] where D was taken as the solute diffusivity of Mg in Al ($D_0 = 5 \times 10^{-5}$ m^2/s and $Q_{sol} = 136$ kJ/mole). The results of these predictive relations were used in constructing deformation mechanism maps for the fine-grained DC and CC-A materials, shown in Figures 7(a) and (b), respectively. The regions over which SRC data were obtained are bounded in Figure 7 by dashed lines. The primary difference between the deformation mechanism maps shown in Figure 7 is a depression of the PLB-SD and SD-GBS transitions to lower stresses in the CC-A material map (Figure 7(b)).

D. *Creep-Transient Analysis*

The data presented from SRC tests so far only include steady-state behaviors, where flow stress is measured after stabilizing at a new strain rate. The transients in flow stress that occur after rate changes in the SRC or TB tests can provide important insight into the deformation mechanisms active under particular test conditions. These transients are particularly important when attempting to identify deformation governed by SD creep, which is suggested by n and Q_c values to occur at high strain rates and low temperatures in the AA5083 materials tested. The SD creep in class I alloys displays a characteristic inverse creep transient.[57,58] The term *inverse* is used because these transients are opposite those displayed by pure metals and class II alloys.[26,58] Upon an increase in strain rate, the flow stress undergoes a large, abrupt increase and then decays toward a steady-state value at the new increased strain rate. Upon a decrease in strain rate, flow stress undergoes a large, abrupt decrease and then gradually increases to a steady-state value at the new reduced strain rate. Such inverse transients are exhibited only by SD creep in class I alloys and, as such, can be used to positively identify the presence of this deformation mechanism. Data from a TB test and from a SRC test are presented as true flow stress *vs* true strain in Figures 8(a) and (b), respectively, for material DC-A tested at 475 °C. The steps at fast strain rates, which correspond to high flow stresses, clearly illustrate inverse transients, which are emphasized in Figure 8 by gray curves fit to the transients. These are conclusive proof that SD creep does control deformation at these rates; the n and Q_c values alone could not be considered conclusive. The absence of transients in steps at slow strain rates is consistent with deformation controlled

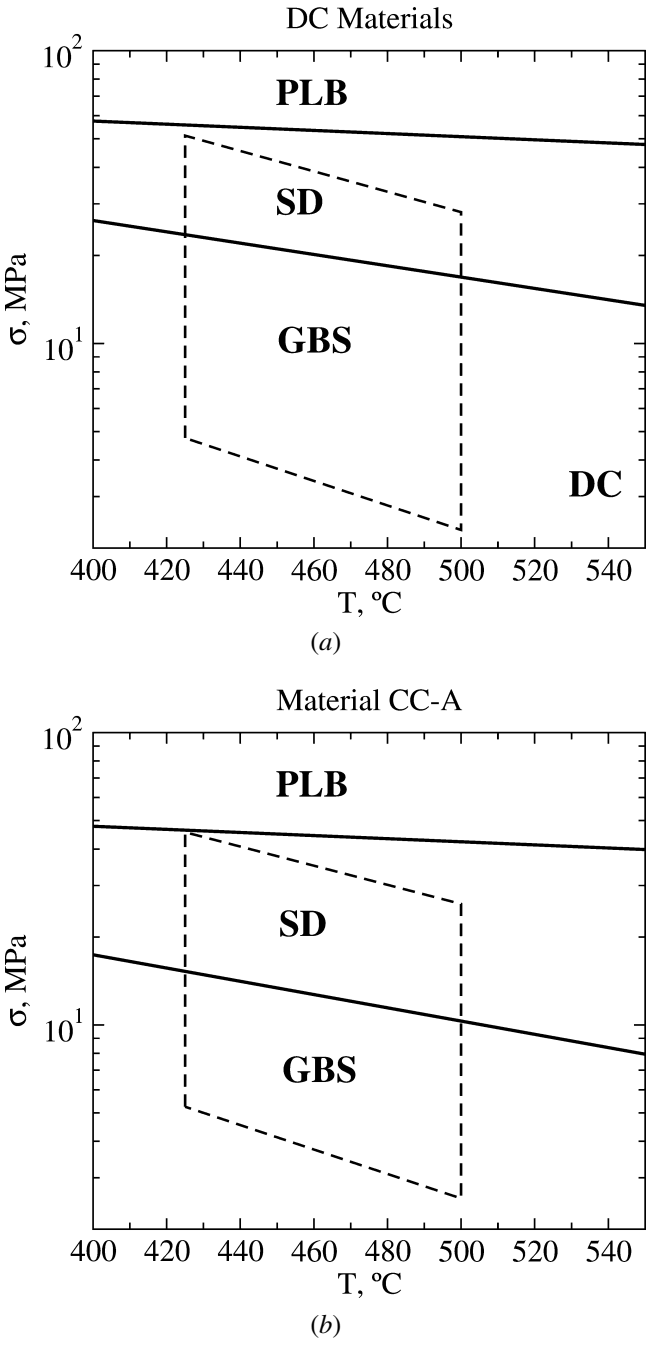

Fig. 7—Deformation mechanism maps are shown as the logarithm of true stress *vs* temperature for (*a*) the fine-grained DC materials and (*b*) the CC-A material. The region within which data were obtained is indicated by a dashed quadrilateral in each plot.

by GBS creep. Data from the TB test shown in Figure 8(a) indicate a clear transient upon the rate increase to a fast rate, where SD creep governs deformation, but shows only a negligible transient upon the subsequent change to a slow rate, where GBS creep controls deformation.

A quantitative analysis of stress transients produced in the AA5083 materials upon changes in strain rate was completed using data from both TB and SRC tests. Quantitative evaluation of stress transients, such as those shown in Figure 8, requires determination of a governing equation for the observed behavior. In developing such an equation, the flow stress after

a rate change was assumed equal to the sum of the steady-state stress at the new strain rate, σ_{ss}, and a transient stress, σ_{tr}, which decays following the rate change. Because SRC and TB tests were conducted for the present investigation using constant crosshead rates, after each rate change, there was a gradual decay in true-strain rate with increasing strain. By using the phenomenological equation for creep, Eq. [2], to relate flow stress to strain rate, the following relationship was derived for rate steps taken at constant crosshead speeds,

$$\sigma_{ss}(\varepsilon) = \sigma_{ss,0} \exp(-\varepsilon/n) \quad [5]$$

where $\sigma_{ss,0}$ is the steady-state flow stress immediately after the rate change, before strain rate decreases from specimen elongation, and ε is the plastic true strain accumulated after the rate change. Because the strain accumulated during each step was small, the variations in $\dot{\varepsilon}$ and σ_{ss} were also small within each step. The rate of decay of the transient stress, σ_{tr}, was discovered to be approximately exponential with strain after a rate change. This dependence can be seen rather clearly in Figure 8(b), wherein stress transients decay at approximately the same rate with strain following each rate change, despite the significantly longer times required for the steps taken at slow rates, *i.e.*, transient decay is strain controlled and independent of time. The exponential decay of the transient stress is represented as follows:

$$\sigma_{tr}(\varepsilon) = \Delta\sigma \exp(-\varepsilon/\tau) \quad [6]$$

where $\Delta\sigma$ is the size of the stress transient immediately following the rate change, ε is as in Eq. [5], and τ describes the rate of decay in the stress transient. Combining Eqs. [5] and [6] provides the following predictive equation for flow stress following a rate change:

$$\sigma_2(\varepsilon) = \sigma_{ss,0} \exp(-\varepsilon/n) + \Delta\sigma \exp(-\varepsilon/\tau) \quad [7]$$

A subscript of 2 in Eq. [7] indicates the flow stress at a new strain rate, $\dot{\varepsilon}_2$, which follows steady-state deformation with a flow stress of σ_1 at a previous strain rate of $\dot{\varepsilon}_1$. Because n was calculated from SRC test data, fitting of Eq. [7] to stress-transient data involves three fitting parameters: $\sigma_{ss,0}$, $\Delta\sigma$, and τ. For transients that occurred primarily under the control of SD creep, as predicted by Figure 7, the value of n was taken as 3.7 by averaging the corresponding measurements in Figure 3. (This n value is slightly different from that shown in the fitted parameters of Table III.) The gray curves in Figure 8 are from fits of Eq. [7] to the corresponding transient data.

Equation [7] was fit to a variety of stress-transient data from SRC and TB tests. The results of fits to experimental data from material DC-C at temperatures of 450 °C and 425 °C are presented in Tables IV and V, respectively. Data

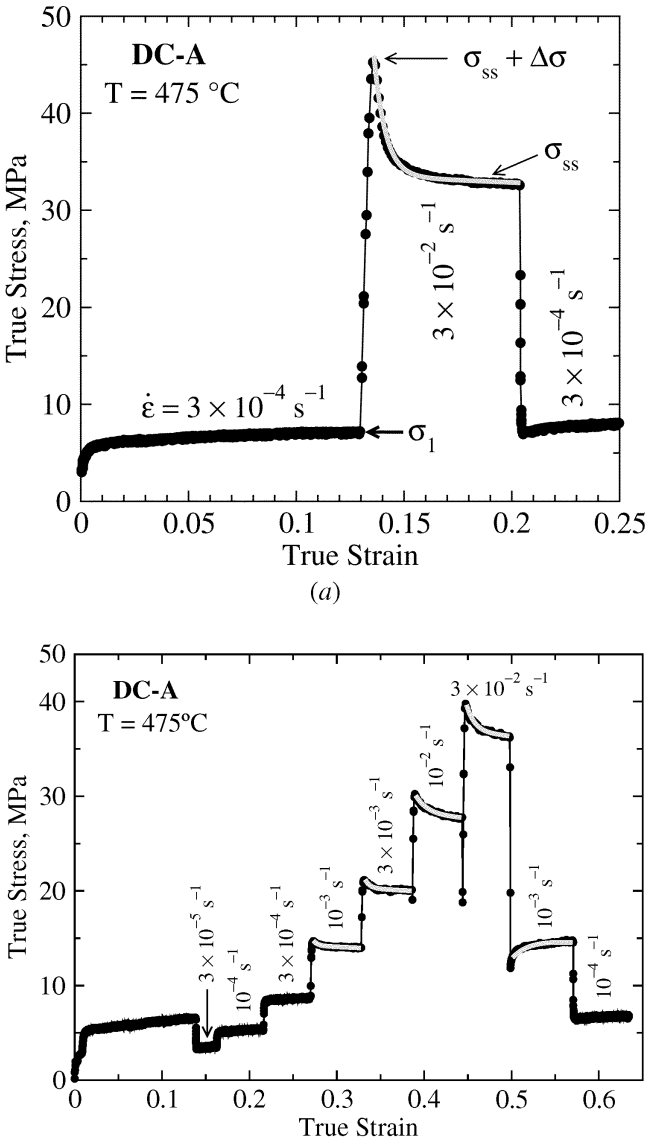

Fig. 8—Transients characteristic of SD creep are shown in data from (*a*) a TB test and (*b*) an SRC test. These data are from material DC-A tested at 475 °C.

Table IV. Transient Behavior Parameters for Material DC-C Tested at 450 °C

$\dot{\varepsilon}_1$ (s^{-1})	σ_1 (MPa)	$\dot{\varepsilon}_2$ (s^{-1})	$\sigma_{ss,SRC}$ (MPa)	$\sigma_{ss,0}$ (MPa)	$\Delta\sigma$ (MPa)	τ
1×10^{-3}	15	3×10^{-3}	25	23	1.4	0.010
3×10^{-3}	23	1×10^{-2}	33	32	3.6	0.012
1×10^{-2}	32	3×10^{-2}	41	42	4.2	0.012
1×10^{-3}	16	5×10^{-3}	28	28	1.6	0.008
1×10^{-3}	15	1×10^{-2}	33	32	4.4	0.007
1×10^{-3}	16	3×10^{-2}	41	44	6.1	0.012
1×10^{-3}	17	5×10^{-2}	44	49	8.8	0.033
*1×10^{-3}	17	1×10^{-1}	49	56	8.5	0.071
3×10^{-3}	23	1×10^{-3}	17	17	−1.4	0.090
5×10^{-3}	28	1×10^{-3}	17	18	−1.3	0.032
1×10^{-2}	32	1×10^{-3}	17	17	−2.1	0.034
3×10^{-2}	42	1×10^{-3}	17	17	−3.2	0.022
5×10^{-2}	46	1×10^{-3}	17	17	−3.9	0.017
*1×10^{-1}	52	1×10^{-3}	17	18	−4.7	0.025

*power-law breakdown occurs

Table V. Transient Behavior Parameters for Material DC-C Tested at 425 °C

$\dot{\varepsilon}_1$ (s^{-1})	σ_1 (MPa)	$\dot{\varepsilon}_2$ (s^{-1})	$\sigma_{ss,SRC}$ (MPa)	$\sigma_{ss,0}$ (MPa)	$\Delta\sigma$ (MPa)	τ
1×10^{-3}	20	3×10^{-3}	29	29	2.5	0.013
3×10^{-3}	29	1×10^{-2}	39	40	4.2	0.016
1×10^{-2}	39	3×10^{-2}	51	52	6.8	0.012
3×10^{-2}	51	1×10^{-3}	20	21	−5.0	0.012

from repeated tests were averaged to produce the values reported. The first two columns in these tables present the initial strain rate, $\dot{\varepsilon}_1$, and steady-state flow stress, σ_1, prior to the rate change that produced the analyzed transient. Equation [7] was fit to the stress transient following a change to rate $\dot{\varepsilon}_2$. The fitting parameter $\sigma_{ss,0}$ is expected to equal the steady-state flow stress at $\dot{\varepsilon}_2$; values of the steady-state flow stress from SRC tests, $\sigma_{ss,\mathrm{SRC}}$, at approximately the same strain rates as shown in the $\dot{\varepsilon}_2$ column are reported in each table for comparison. These two independent measurements are in very close agreement, which supports the validity of the fits to transient data. The stress-transient sizes, $\Delta\sigma$, reported in Tables IV and V increase with the size of strain-rate changes. The decay constant, τ, shows significant variability between data sets. No clear changes in τ with temperature are evident. Considering the variation in τ values from repeated tests, the approximate range of τ values is 0.01 to 0.04. Two of the data sets presented in Table IV fall into the early portion of the PLB region of deformation (Figure 7), and these tests are noted in Table IV. In summary, Tables IV and V indicate that the fitting parameter $\sigma_{ss,0}$ agrees closely with independently measured values of steady-state flow stress, $\sigma_{ss,\mathrm{SRC}}$, and that the decay constant, τ, is essentially constant to within the error in measurements.

The relative sizes of stress transients are analyzed using the graphical construction demonstrated in Figure 9. In this construction, the logarithm of the ratios of flow stresses before and after the rate change, $\log(\sigma_2/\sigma_1)$, are plotted against the logarithm of the ratios of the strain rates before and after the rate change, $\log(\dot{\varepsilon}_2/\dot{\varepsilon}_1)$. The values of stress and strain rate assume that steady-state flow is achieved prior to any change. For a strain-rate change, the strain rate after the change, $\dot{\varepsilon}_2$, is a constant. The flow stress after the change, σ_2, varies with strain. For the purposes of this graphical construction, the two extreme values of are plotted. These are the stress immediately after the rate change, $\sigma_2 = \sigma_{ss,0} + \Delta\sigma$, and the steady-state stress, $\sigma_2 = \sigma_{ss,0}$, following the rate change. Fitting of Eq. [7] to transient data provides a convenient means of determining the stress immediately following a rate change, as it is problematic to directly measure this quantity. The steady-state values of stress and strain rate for changes within the governance of a single deformation mechanism will produce a straight line that passes through the origin of the construction axes. Furthermore, the slope of these steady-state data will equal the strain-rate sensitivity, m, which is the inverse of the stress exponent in Eq. [2], *i.e.*, $m = 1/n$. This line is called the steady-state line. Plotting data of the stresses immediately following rate changes will also produce a straight line passing through the construction origin; this line is called the transient line. As this result is not predicted from theory for the case of SD creep,[59–62] it will be proved in Figure 10 using experimental data. Thus, the graphical construction of Figure 9 provides a model by which the size of creep transients is predicted relative to steady-state behavior.

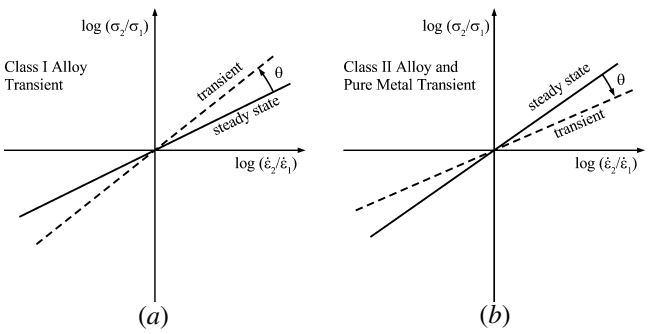

Fig. 9—Schematics of graphical constructions for representing transient creep behaviors in (*a*) class I alloys and (*b*) class II alloys and pure metals are shown.

The difference between the relative transient and steady-state stresses is represented in Figure 9 by a rotation of the transient line from the steady-state line. The angle of this rotation is a measure of the relative size of transients under the governing deformation mechanism. If the transient line is plotted using $\sigma_2(\varepsilon)$, then the angle θ will decrease with strain, reflecting the decay of the transient, until the transient line returns to the steady-state line; this aspect of the proposed graphical construction is not further investigated for this study. For the inverse transients of SD creep, the transient line is rotated counterclockwise from the equilibrium line, as shown in Figure 9(a). The normal transients of creep in pure metals and class II alloys will produce a transient line rotated clockwise from the equilibrium line, as shown in Figure 9(b). For pure metals, the steady-state line will have a slope of 1/5 and the transient line will have a slope of 1/8, according to the theory of constant-structure creep.[63] The proposed graphical construction, thus, provides a clear representation of both class I and class II creep transient behaviors. Furthermore, it can be used for data from both SRC experiments and stress-change experiments. For stress-change experiments, the stress prior to the imposed stress change is σ_1, which produces a corresponding steady-state strain rate of $\dot{\varepsilon}_1$, and the stress imposed after the change is σ_2. The steady-state line is then produced using $\dot{\varepsilon}_2$ equal to the steady-state strain rate following the change. The transient line is produced using $\dot{\varepsilon}_2$ equal to the plastic strain rate immediately following the stress change. These values can be calculated by fitting transient data in a manner reminiscent of the method described previously for SRC data.

The SRC and TB test data of material DC-C at 450 °C, provided in Table IV, are plotted in Figure 10(a) according to the graphical construction shown in Figure 9. It is of note that the data from small, positive rate jumps show the most deviation from linearity. The slope of the steady-state line in Figure 10(a) is $m = 0.27$, which is consistent with the stress exponents reported in Figure 3. The transient data clearly form a single line, as described previously, with a slope of 0.32, and this line is rotated counterclockwise from the steady-state line. The measured value of θ is 2.6 deg. The data for the largest jump sizes deviate from linear behavior. This is because of intervention by PLB, as indicated in Table IV for these data. The lines of Figure 10(a) were fit to the remaining data by linear regression. The deviation from linearity because of PLB is represented approximately by curves at the ends of the linear regions. These same curves are repeated in Figure 10(b), which contains data from the DC-C material tested at 425 °C. The data taken at 425 °C clearly fall along the lines fit to the 450 °C data, indicating an absence of temperature dependence in this representation of the transient behaviors. Limited data for small, positive strain-rate changes from the DC-C material at 475 °C and 500 °C and from the DC-A material at 450 °C and 475 °C

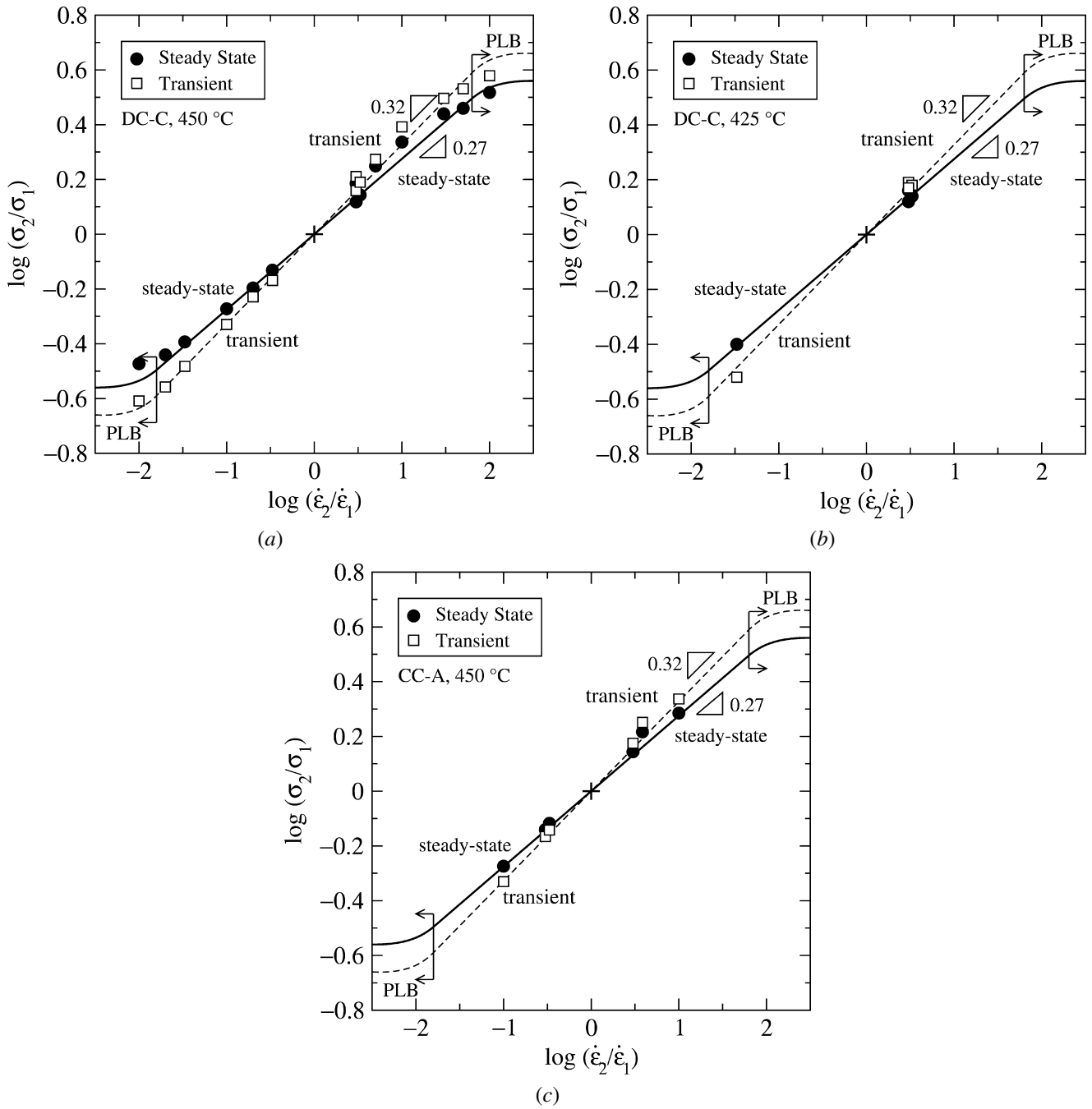

Fig. 10—Graphical constructions for the analysis of creep transients are shown for material DC-C at (*a*) 450 °C and (*b*) 425 °C and (*c*) for material CC-A at 450 °C.

show similar agreement with the lines fit to DC-C data at 450 °C. Thus, this graphical representation reveals that the relative size of stress transients under SD creep are independent of temperature, *i.e.*, the temperature dependence is wholly contained in the steady-state $\dot{\varepsilon}$-σ relationship, as in Eq. [2]. The curves from Figure 10(a) are repeated again in Figure 10(c), which presents data from material CC-A tested at 450 °C; these data are plotted from those presented in Table VI, for which data from tests using identical strain-rate changes were averaged. The CC-A data fall along the curves produced from DC-C data, indicating that transient behaviors in these two materials are very nearly the same.

Table VI. Transient Behavior Parameters for Material CC-A Tested at 450 °C

$\dot{\varepsilon}_1$ (s^{-1})	σ_1 (MPa)	$\dot{\varepsilon}_2$ (s^{-1})	$\sigma_{ss,SRC}$ (MPa)	$\sigma_{ss,0}$ (MPa)	$\Delta\sigma$ (MPa)	τ
2.6×10^{-3}	17	1×10^{-2}	29	28	2.3	0.012
1×10^{-2}	28	3×10^{-2}	37	39	2.9	0.013
3×10^{-3}	21	3×10^{-2}	37	41	4.7	0.010
3×10^{-3}	21	3×10^{-2}	37	40	5.5	0.010
3×10^{-2}	38	1×10^{-2}	29	29	−1.6	0.030
1×10^{-2}	29	3×10^{-3}	21	21	−1.2	0.020
3×10^{-2}	39	3×10^{-3}	21	21	−2.4	0.011
3×10^{-2}	38	3×10^{-3}	21	20	−2.6	0.014

Data are available from Mills *et al*. for creep transients in low-impurity Al-Mg at temperatures of 300 °C and 400 °C.[64] The Al material in these studies contained 5.5 at. pct Mg. Mills *et al*. completed a campaign of stress-drop experiments at 300 °C and 400 °C on this material,[64] and their data were extracted to be analyzed in the manner of Figures 9 and 10. Figures 11(a) and (b) contain the data from Mills *et al*. at temperatures of 300 °C and 400 °C, respectively. Steady-state values are plotted in Figures 11(a) and (b) by simply taking the differences in stress and strain rate between any two independently determined steady-state data points reported at a single temperature. The steady-state lines in Figures 11(a) and (b) are identical and were fit by regression to all the values from steady-state data at both 300 °C and 400 °C simultaneously. These clearly show no dependence on temperature. The slope of the steady-state line is 0.32, which is consistent with the stress exponents measured by Mills *et al*., which ranged from 3.0 to 3.2. The transient data at both 300 °C and 400 °C were also used simultaneously to fit a single transient line, which is shown in both Figures 11(a) and (b). The slope of this transient line is 0.48, and it is rotated counterclockwise from the steady-state line. The measured value of θ is 7.9 deg, which is greater than that measured for the AA5083 materials. The transient lines in Figures 11(a) and (b) do not exhibit any temperature dependence, which is consistent with data from AA5083 materials of the present study. From Figures 10 and 11, it is concluded that the relative sizes of SD creep transients are independent of temperature. Comparing Figure 10 with Figure 11 makes it clear that the slopes of both the steady-state and transient lines depend on the material. This material dependence is consistent with the increase in stress exponent observed when Mn and other additions typical of commercial 5000-series aluminum alloys are made to low-impurity Al-Mg materials.[25,34,65,66]

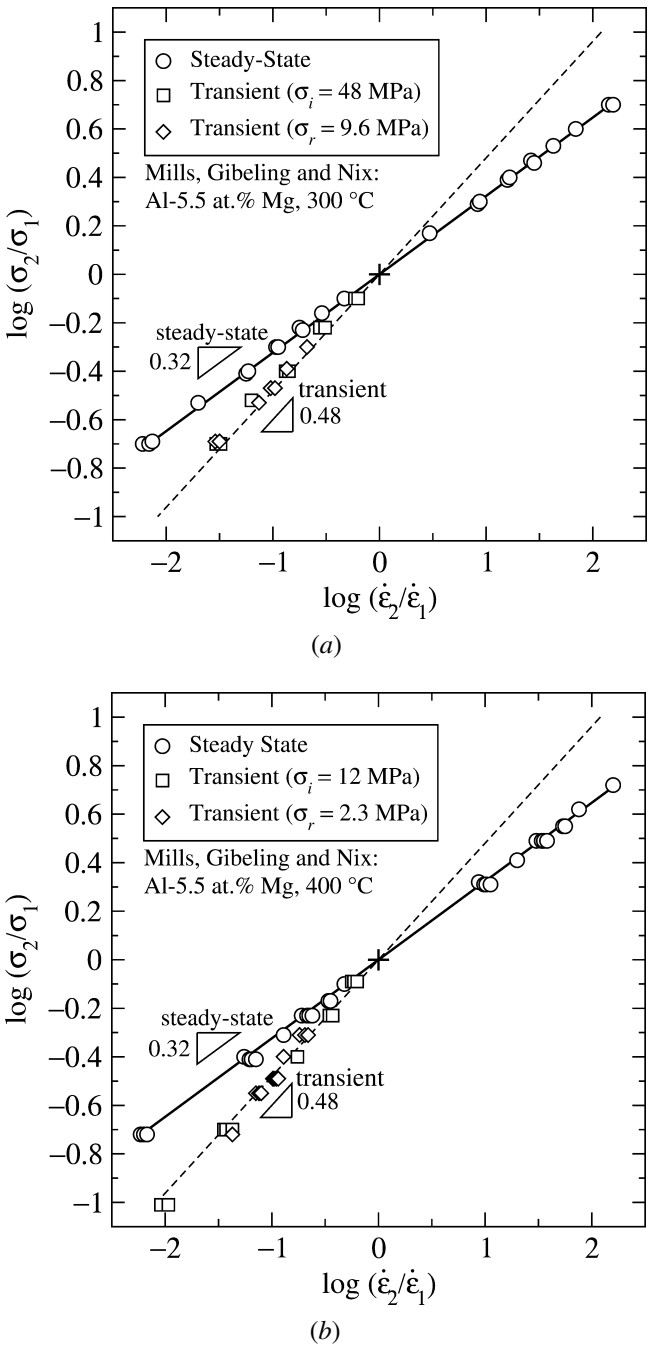

Fig. 11—Graphical constructions for the analysis of creep transients are shown for the Al-Mg material of Mills *et al*.[64] at (*a*) 300 °C and (*b*) 400 °C.

IV. CONCLUSIONS

Mechanical testing and optical microscopy were used to characterize the deformation behaviors of seven AA5083 materials from five alloy heats over a range of strain rates and temperatures. All the fine-grained AA5083 materials produced stress exponents and activation energies characteristic of GBS creep at high temperatures and slow strain rates. Stress exponents and creep activation energies measured at low temperatures and fast strain rates are characteristic of deformation by SD creep. Furthermore, an analysis of stress transients following strain-rate changes proves conclusively that these materials deform by SD creep under these conditions. The single coarse-grained AA5083 material investigated deformed by SD creep throughout the range of temperatures and strain rates studied. Deformation mechanism maps characterizing deformation in the fine-grained AA5083 materials were constructed. The similarity in deformation mechanisms and flow stresses between the fine-grained AA5083 materials makes it unlikely that differences in ductility between these materials in hot-forming operations are associated with differences in active deformation mechanisms. Pronounced stress transients following strain-rate changes were measured in the AA5083 materials for deformation in the SD creep regime. It was discovered that these stress transients decay approximately exponentially with strain, with no observed time dependence. These transients were analyzed using a new graphical methodology. The resulting graphical construction reveals relative transient size to be independent of temperature; temperature dependence resides in the steady-state relations. The methodology developed is the first to allow general prediction of the size and duration of SD creep transients that arise from either strain-rate or stress changes. The transient behavior of low-impurity, binary Al-Mg material differs from that of the commercial AA5083 materials, which is consistent with the difference previously observed between low-impurity and commercial Al-Mg alloys under steady-state creep conditions.

ACKNOWLEDGMENTS

The authors gratefully acknowledge support from the General Motors Corp. for this work.

REFERENCES

1. A. Kelkar, R. Roth, and J. Clark: *JOM*, 2001, vol. 53, pp. 28-32.
2. J.G. Schroth: in *Advances in Superplasticity and Superplastic Forming*, E.M. Taleff, P.A. Friedman, P.E. Krajewski, R.S. Mishra, and J.G. Schroth, eds., TMS, Warrendale, PA, 2004, pp. 9-20.
3. K. Osada and K. Shirkawa: in *Advances in Superplasticity and Superplastic Forming*. E.M. Taleff, P.A. Friedman, P.E. Krajewski, R.S. Mishra, and J.G. Schroth, eds., TMS, Warrendale, PA, 2004, pp. 41-49.
4. P.E. Krajewski: in *Advances in Superplasticity and Superplastic Forming*, E.M. Taleff, P.A. Friedman, P.E. Krajewski, R.S. Mishra, and J.G. Schroth, eds., TMS, Warrendale, PA, 2004, pp. 173-83.
5. O.D. Sherby and J. Wadsworth: *Progr. Mater. Sci*., 1989, vol. 33, pp. 169-221.
6. A. Ball and M.M. Hutchison: *Met. Sci. J*., 1969, vol. 3, pp. 1-7.
7. O.D. Sherby and J. Wadsworth: in *Deformation, Processing, and Structure*, G. Kraus, ed., ASM, Metals Park, OH, 1982, pp. 355-89.
8. T. G. Langdon: *Metall. Trans. A*, 1982, vol. 13A, pp. 689-701.
9. A. Arieli and A.K. Mukherjee: *Metall. Trans. A*, 1982, vol. 13A, pp. 717-32.
10. J.W. Edington: *Metall. Trans. A*, 1982, vol. 13A, pp. 703-15.
11. G.S. Murty and M.J. Koczak: *Mater. Sci. Eng*., 1987, vol. 96, pp. 117-24.
12. O.D. Sherby and J. Wadsworth: in *Superplasticity in Aerospace*, H.C. Heikkenen and T.R. McNelley, eds., TMS, Warrendale, PA, 1988, pp. 3-27.
13. H. Fukuyo, H.C. Tsai, T. Oyama, and O.D. Sherby: *Iron Steel Inst. Jpn. Int*., 1991, vol. 31, pp. 76-85.
14. T.G. Langdon: *Mater. Sci. Eng*., 1991, vol. A137, pp. 1-11.
15. T.G. Nieh, J. Wadsworth, and O.D. Sherby: *Superplasticity in Metals and Ceramics*, Cambridge University Press, Cambridge, United Kingdom, 1997, pp. 58-69.
16. J.S. Vetrano, C.A. Lavender, C.H. Hamilton, M.T. Smith, and S.M. Bruemmer: *Scripta Metall*., 1994, vol. 30, pp. 565-70.
17. Y. Takayama, S. Sasaki, T. Tozawa, H. Kato, H. Watanabe, and M. Kokubo: *J. Jpn. Inst. Light Met*., 1999, vol. 49, pp. 378-82.
18. D.H. Bae and A.K. Ghosh: *Acta Mater*., 2000, vol. 48, pp. 1207-24.
19. I.C. Hsiao and J.C. Huang: *Metall. Mater. Trans. A*, 2002, vol. 33A, pp. 1373-84.
20. R.M. Cleveland, A.K. Ghosh, and J.R. Bradley: *Metall. Mater. Trans. A*, 2003, vol. 34A, pp. 228-36.
21. P.A. Friedman and W.B. Copple: in *Hot Deformation of Aluminum Alloys III*, Z. Jin, A. Beaudoin, T.A. Bieler, and B. Radhakrishnan, eds., TMS, Warrendale, PA, 2003, pp. 211-19.
22. C.F. Martin, J.J. Blandin, and L. Salvo: *Mater. Sci. Eng*., 2001, vol. 297, pp. 212-22.
23. M.-A. Kulas, P.E. Krajewski, T.R. McNelley, and E.M. Taleff: in *Hot Deformation of Aluminum Alloys III*, Z. Jin, A. Beaudoin, T. Bieler, and B. Radhakrishnan, eds., TMS, Warrendale, PA, 2003, pp. 499-507.
24. M.-A. Kulas, W.P. Green, E.C. Pettengill, P.E. Krajewski, and E.M. Taleff: in *Advances in Superplasticity and Superplastic Forming*, E.M. Taleff, P.A. Friedman, P.E. Krajewski, R.S. Mishra, and J.G. Schroth, eds., TMS, Warrendale, PA, 2004, pp. 127-38.
25. E.M. Taleff: in *Advances in Superplasticity and Superplastic Forming*, E.M. Taleff, P.A. Friedman, P.E. Krajewski, R.S. Mishra, and J.G. Schroth, eds., TMS, Warrendale, PA, 2004, pp. 85-94.
26. F.A. Mohamed and T.G. Langdon: *Acta Metall*., 1974, vol. 22, pp. 779-88.
27. F.A. Mohamed: *Scripta Metall*., 1978, vol. 12, pp. 99-102.
28. P. Yavari and T.G. Langdon: *Acta Metall*., 1982, vol. 30, pp. 2181-96.
29. P. Yavari, F.A. Mohamed, and T.G. Langdon: *Acta Metall*., 1981, vol. 29, pp. 1495-1507.
30. H.J. McQueen and M.E. Kassner: in *Superplasticity in Aerospace II*, T.R. McNelley and H.C. Heikkenen, eds., TMS, Warrendale, PA, 1990, pp. 189-206.
31. G.A. Henshall, M.E. Kassner, and H.J. McQueen: *Metall. Trans. A*, 1992, vol. 23A, pp. 881-89.
32. E.M. Taleff, D.R. Lesuer, and J. Wadsworth: *Metall. Mater. Trans. A*, 1996, vol. 27A, pp. 343-52.
33. E.M. Taleff, G.A. Henshall, T.G. Nieh, D.R. Lesuer, and J. Wadsworth: *Metall. Mater. Trans. A*, 1998, vol. 29A, pp. 1081-91.
34. E.M. Taleff, P.J. Nevland, and P.E. Krajewski: *Metall. Mater. Trans. A*, 2001, vol. 32A, pp. 1119-30.
35. J. Wang, Z. Horita, M. Furukawa, M. Nemoto, N.K. Tsenev, R.Z. Valiev, Y. Ma, and T.G. Langdon: *J. Mater. Res*., 1993, vol. 8, pp. 2810-18.
36. K. Kannan, J.S. Vetrano, and C.H. Hamilton: *Metall. Mater. Trans. A*, 1996, vol. 27A, pp. 1947-57.
37. J.S. Vetrano, S.M. Bruemmer, L.M. Pawlowski, and I.M. Robertson: *Mater. Sci. Eng*., 1997, vol. A238, pp. 101-07.
38. J.S. Vetrano, J. Henager, H. Chuck, S.M. Bruemmer, Y. Ge, and C.H. Hamilton: in *Superplasticity and Superplastic Forming*, A.K. Ghosh and T.R. Bieler, eds., TMS, Warrendale, PA, 1998, pp. 89-98.
39. L.M. Dougherty, I.M. Robertson, and J.S. Vetrano: *Mater. Res. Soc. Symp. Proc*., 2000, vol. 601, pp. 25-30.
40. T. Aiura, N. Sugawara, and Y. Miura: *Mater. Sci. Eng*., 2000, vol. 280A, pp. 139-45.
41. J.S. Vetrano, C.A. Lavender, and S.M. Bruemmer: in *Superplasticity and Superplastic Forming*, A.K. Ghosh and T.R. Bieler, eds., TMS, Warrendale, PA, 1995, pp. 49-56.
42. J.S. Vetrano, C.H. Henager, and V.Y. Guertsman: in *Advances in Superplasticity and Superplastic Forming*, E.M. Taleff, P.A. Friedman, P.E. Krajewski, R.S. Mishra, and J.G. Schroth, eds., TMS, Warrendale, PA, 2004, pp. 225-32.
43. J.S. Vetrano, D.R. Baer, and R.H. Jones: in *Automotive Alloys II*, S.K. Das, ed., TMS, Warrendale, PA, 1998, pp. 117-23.
44. D.O. Sprowls and R.H. Brown: in *Fundamental Aspects of Stress Corrosion Cracking*, NACE, Houston, TX, 1969, pp. 466-512.
45. *ASTM. Standard Designation E 112-96*, ASTM, West Conshohocken, PA, 1996.
46. W. Köster: *Z. Metallkd*., 1948, vol. 39, pp. 1-9.
47. P.K. Chaudhury and F.A. Mohamed: *Acta Metall*., 1988, vol. 36, pp. 1099-1110.
48. C.R. Barrett, A.J. Ardell, and O.D. Sherby: *Trans. ASM*, 1964, vol. 230, pp. 200-04.
49. R. Horiuchi and M. Otsuka: *Trans. JIM*, 1972, vol. 13, pp. 284-93.
50. K.L. Murty, F.A. Mohamed, and J.E. Dorn: *Acta Metall*., 1972, vol. 20, pp. 1009-18.
51. H. Oikawa, J. Kariya, and S. Karashima. *Met. Sci*., 1974, vol. 8, pp. 106-11.
52. H. Oikawa, N. Matsuno, and S. Karashima: *Met. Sci*., 1975, vol. 9, pp. 209-12.
53. J.W. Harrell: Master's Thesis, Naval Postgraduate School, Monterey, CA, 2001.
54. T.A. Maestas: Master's Thesis, Naval Postgraduate School, Monterey, CA, 2002.
55. H.J. Frost and M.F. Ashby: *Deformation-Mechanism Maps*, Pergamon Press Inc., New York, NY, 1982, pp. 1-19.
56. T.G. Nieh, J. Wadsworth, and O.D. Sherby: *Superplasticity in Metals and Ceramics*, Cambridge University Press, Cambridge, United Kingdom, 1997, pp. 40-53.
57. O.D. Sherby and P.M. Burke: *Progr. Mater. Sci*., 1968, vol. 13, pp. 325-90.
58. W.R. Cannon and O.D. Sherby: *Metall. Trans. A*, 1970, vol. 1, pp. 1030-32.
59. J. Weertman: *J. Appl. Phys*., 1957, vol. 28, pp. 1185-89.
60. J. Weertman: *Trans. TMS-AIME*, 1960, vol. 218, pp. 207-18.
61. W.L. James and D.M. Barnett: in *Solute-Defect Interaction Theory and Experiment*, S. Saimoto, G.R. Purdy, and G.V. Kidson, eds., Pergamon Press, Elmsford, NJ, 1986, pp. 136-42.
62. E.M. Taleff and J. Qiao: *Modeling the Performance of Engineering Structural Materials II*, T. Srivatsan and D.R. Lesuer, eds., TMS, Warrendale, PA, 2001, pp. 3-12.
63. J. Lin and O.D. Sherby: *Res. Mech*., 1981, vol. 2, pp. 251-93.
64. M.J. Mills, J.C. Gibeling, and W.D. Nix: *Acta Metall*., 1985, vol. 33, pp. 1503-14.
65. E.M. Taleff, P.J. Nevland, and S.J. Yoon: in *Deformation, Processing, and Properties of Structural Materials*, E.M. Taleff, C.K. Syn, and D.R. Lesuer, eds., TMS, Warrendale, PA, 2000, pp. 373-84.
66. E.M. Taleff and J. Qiao: *Light Metals 2001—Métaux Légers*, M. Sahoo and T. Lewis, eds., Canadian Institute of Mining, Metallurgy, and Petroleum, Montral, 2001, pp. 77-88.